Soft Computing (2024) 28:8423–8434
https://doi.org/10.1007/s00500-024-09742-8

APPLICATION OF SOFT COMPUTING

Enhanced deep learning model for diagnosing breast cancer using thermal images

N. P. Dharani[1,2] · I. Govardhini Immadi[1] · M. Venkata Narayana[1]

Accepted: 29 January 2024 / Published online: 5 July 2024

Abstract

Breast cancer has emerged as one of the most prevalent malignancies affecting women today, underscoring the critical need for advanced diagnostic tools. Mammography has been the conventional method for early breast cancer detection, yet recent years have witnessed the emergence of thermal infrared scans, or thermographies, as a potential contender for diagnosing breast cancer, particularly in cases of dense breast tissue. Thermographic images reveal higher temperatures in regions containing tumors compared to healthy breast tissue, providing a promising avenue for early diagnosis. In parallel, the field of radiography has seen the advent of deep learning (DL) techniques, offering a computational approach to breast cancer identification. This study presents a novel approach, the Enhanced Deep learning-based Convolutional Neural Network (EDCNN), aimed at generating heatmaps from two-dimensional thermal breast images. These heatmaps are employed to quantitatively assess breast vascularity, yielding interpretable parameters for further analysis. In addition, the study proposes a classifier that predicts the likelihood of breast cancer purely based on these extracted parameters. To enhance the accuracy of this process, the algorithm combines Fuzzy *C*-means clustering with the Region of Interest (ROI) technique to effectively isolate the breast from surrounding body parts. The segmentation results are evaluated using temperature profiles, revealing substantial peaks in the patterns as indicators of ROIs. This identification of hot areas hints at the potential presence of a tumor. To validate the effectiveness of this approach, the study constructs DL models using convolutional neural networks, training them with thermal breast images from the Graphical DMR datasets. The results are compelling, with the EDCNN models outperforming alternative methods, achieving an impressive accuracy of 96.8% and a specificity rate of 93.7%. This research thus offers a robust, efficient, and reliable means of early breast cancer diagnosis, marking a significant advancement in the field.

Keywords Breast cancer · Deep learning · EDCNN · Fuzzy *C*-means · Region of interest · Segmentation · Thermography image

1 Introduction

The breast cancer incidence accounts for thirty percent of all occurrences of cancers and ranks as the second highest mortality rate in women over the age of 30, behind breast cancer (Chatterjee et al. 2022). Researchers in the field of oncology believe that the acceptance of Modern lifestyle among Indian women, namely the practice of delaying childbearing and marriage until later stages of life, is to responsible for the probable outbreak of breast cancer over the upcoming 10 years in India. Breast cancer affects each of every 23 Indian females at some time in their lives (Allugunti 2022). Oncology professionals believe that a woman's hormone levels are more likely to be altered if

✉ N. P. Dharani
dharininp@gmail.com

I. Govardhini Immadi
govardhini456@gmail.com

M. Venkata Narayana
venkatanarayana234@gmail.com

[1] Department of ECE, Koneru Lakshmaiah Education Foundation, Vaddeswaram Guntur, AP, India

[2] Department of ECE, Mohan Babu University (Erstwhile Sree Vidyanikethan Engineering College), Tirupati, India

she has fewer children as well as weans youngsters during an earlier age. This exposes women at such a greater risk of developing breast cancer. According to a research done in 2021, 145,985 women became newly diagnosed with breast cancer, whereas 70,218 women passed away from the disease (Mashekova et al. 2022). This indicates that for every two women who are present in patients diagnosed, one woman passes away. Thermography can furthermore be used again for sooner diagnosis of breast cancer. Breast thermography was already performed in 1956, and it was the initial recorded implementation of infrared (IR) image analysis or thermography in healthcare (Tsietso et al. 2022). At that time, IR images of some breasts of women with breast cancer have been analyzed for non-symmetric points as well as capillary density. Breast thermography is considered to be one of the most accurate methods of diagnosing breast cancer (Al Husaini et al. 2022).

Screening mammography representations have been frequently utilized diagnose breast cancer at an early stage stages; nevertheless, some studies have demonstrated that thermal IR visuals, also recognized as thermographies, could indeed produce significant early screening results in the instance of breast density (Torres-Galvan et al. 2022). This is especially true for women whom have dense breasts. Compared to magnetic resonance imaging (MRI) and mammography treatments, the cost of dynamic thermography is significantly lower (Dar et al. 2022). Furthermore, this is a non-invasive diagnostic procedure that does not hurt patients and does not release any ionizing radiation, making it safe. Two fundamental facts support thermography: first, the surface temperatures of breast cancerous regions are higher than those of the surrounding body tissue; and second, the rates of physiologic heat generation and blood fluid overload in tumors are significantly higher than those in normal regions (Ensafi et al. 2022). It is possible to record the temperature differential between sick and healthy breast tissue using IR light imaging.

The above portraits are being utilized to improve a method for distinguishing among benignity as well as malignancy of breast cancer, and it has been discovered that perhaps the entropy consequences greatly vary among malignant and benign structures (Patra et al. 2022). Highly sensitive IR scanners that keep producing high resolution which initiate IR images. Thermography may address breast cancer in its early stages by analyzing the breast for uneven heat flux in addition to hot or cold regions. This can be done by analyzing the breast.

Using DWT with SVM, it was able to identify mass lesions, and the rate that it attained was 92%. The deep convolution neural networks, also known as the DCNN, was used for the mass detection in this study (Ragab et al. 2022). The DCNN was given its first taste of transfer learning thanks to this work. By using data dictionary for mammography screening, the accuracy attained for distinguishing between normal lesions versus masses was 89.9%. However, breast cancer becomes widespread health concern, yet existing diagnostic methods are not always accurate or efficient, particularly in region with limited access to healthcare. The study motivation for this research is to provide a solution to this critical problem by developing an advanced diagnostic system using thermal images. This system's efficiency reliability and enhanced accuracy empower healthcare professionals in early detection of breast cancer, addressing the urgent need for improved diagnostic tools, particularly in underserved areas. Our contributions are,

1. develops a cutting-edge breast cancer diagnostic system for more accurate and reliable early detection.
2. dignificantly enhances diagnostic accuracy, making it a valuable tool for healthcare professionals in breast cancer identification.
3. boosts efficiency and reliability through the EDCNN, offering both faster and more robust early breast cancer detection using thermal imaging.

2 Thermal images to predict breast cancer

The datasets were obtained using the DMR (database for mastology research) (Ahmed 2022). We utilized thermal photos of the breasts taken from the front, to the left 45°, to the right 45°, to the left 90°, and to the right 90° (Mishra et al. 2020). Following the acquisition of thermal pictures and clinical data, we proceeded to data and image preparation. We gathered pictures with dimensions around 640 × 480. Patients whose images were unclear, did not complete procedure, as well as did not get all five perspectives were excluded as from datasets. Any unusual items were also removed during data preparation (Hakim and Awale 2020). The EDCNN model's implementation in MATLAB involved specific parameters crucial for its effectiveness. EDCNN could only process square images, to meet this prerequisite; the thermal images originally of varying dimensions, were uniformly resized to 640 × 640 pixels. This standardization ensured data uniformity and compatibility for the EDCNN model, enabling consistent and efficient image analysis and classification. MATLAB's has image processing capabilities converting each image to the square format. By adhering to these parameters, the model was not only prepared for optimal performance but also proficient in diagnosing breast cancer using thermal images while maintaining the square image requirements (Table 1).

Table 1 Existing works on breast cancer diagnosis

Study	Methodology	Results
Chatterjee et al. (2022)	Grunwald–Letnikov (GL) method	82% accuracy
Allugunti (2022)	Convolutional neural network (CNN)	89.84% accuracy
Tsietso et al. (2022)	Deep neural networks (DNNs)	95.8% accuracy
Dar et al. (2022)	Modified inception MV4	High accuracy, sensitivity, specificity, positive predictive value, equal error rate and $F1$ score
Ensafi et al. (2022)	Deep convolutional neural network (CNN)	Sensitivity of 92.3% and a specificity of 53.8%
Patra et al. (2022)	Deep learning and deep reinforcement learning	Not applicable
Ragab et al. (2022)	Applied deep learning	Sensitivity increase of 2–15% and a specificity increase of 2–30%

Although breast cancer continues to be the most frequent type of cancer in women, many countries do not have access to screening tools that can determine a woman's cancer state. In general, the suggested system comprises of the following steps: (1) pre-processing as well as enhancement, (2) image segmentation, (3) feature extraction of an image, (4) EDCNN classifications, and (5) performance evaluation (Fig. 1).

2.1 Pre-processing

Thermal pictures need extensive pre-processing before being sent through into DCNN. It automates the removal of undesired parts such as the underarm, wrists, shoulders, as well as belly (Zadeh et al. 2016). Furthermore, while passing a thermal picture into a separate EDCNN, the image size must be appropriately adjusted. Pre-processing is among the fundamental steps of breast cancer diagnosis in which the picture is resized, the backdrop is removed, and unwanted body parts are removed, followed by normalisation as well as pattern classification of the image by binarization.

An input image may be transformed from RGB toward greyscale, and all images were resized to 640 × 640 before using an adaptive median filter to remove noisy pixels, as illustrated in Fig. 2.

To increase the viability of evaluating the pictures individually in the EDCNN analysis, image pre-processing implies the procedures needed to make images from various sources more compatible.

The primary function of the pre-processing stage is to do the segmented data, which entails locating the ROI in each picture and isolating it away from rest of the frame. This is done during the step known as pre-processing.

2.1.1 Image enhancement

The inability to see fine details and minor changes in an image due to low contrast can have an impact on the interpretation of IR pictures. The concept can be demonstrated with the greyscale picture in Fig. 3 (Sánchez-Cauce et al. 2021). In this instance, the image's low contrast is the primary reason why the thermal pattern display is subpar. Examining the intensity histogram on the provided image makes it simple to verify this information.

Pixels from the chest area of the group having higher peak values at the lowest pixel value can be utilized to transform the binary image into an improved version. However, each picture has this feature of a clear contrast in

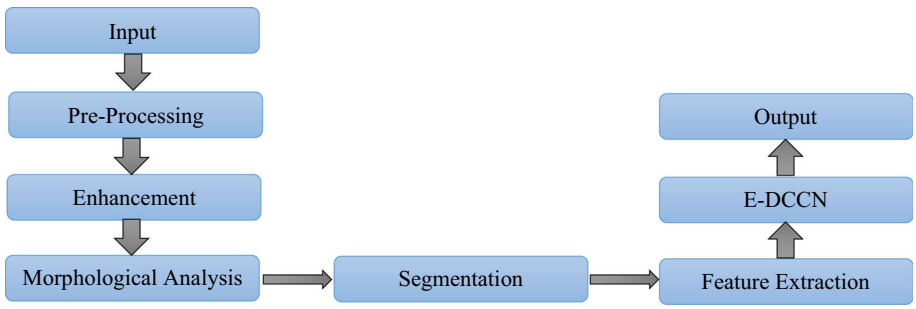

Fig. 1 Steps for predicting breast cancer

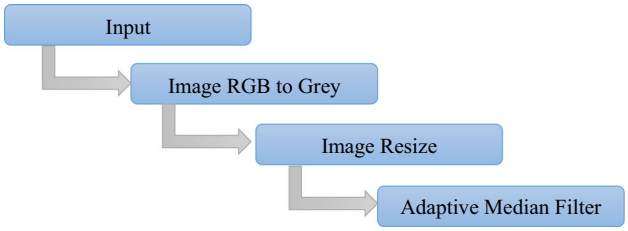

Fig. 2 Pre-processing techinque

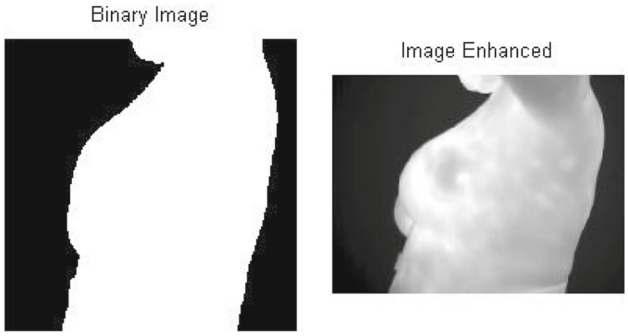

Fig. 3 Image enhancement

intensity between the background and the breast area (Karthiga and Narasimhan 2021). Scaling the chest region's pixel distribution to encompass the whole intensity range can improve these images.

2.2 Segmentation

The technique of dividing an image into sections that each include subparts that share similar qualities and characteristics is known as image segmentation. The basic objective of segmentation is help to reduce the number of images by presenting them in a format that can be examined more easily (Darabi et al. 2021). Edge detection, based on fuzzy, partial differential equation (PDE), artificial neural network (ANN), thresholds value, as well as region-based segmentation are among the most prominent picture segmentation approaches as shown in Fig. 4.

2.2.1 Fuzzy *C*-means clustering

Based on a clustering technique that separates a data set into N groups, Fuzzy *C*-means (FCM) assigns varied degrees of membership to each cluster to each data source within datasets. For instance, a data point located in the center of a cluster will have a high percentage of inclusion in that cluster, but a data point located further from the center of a cluster will have a lower degree of engagement.

Steps for fuzzy *C*-means clustering as given below,

```
maximum C = maximum (C);
indexing = units (N,1);
for
{
i = N:1
}
    indexing{i} = locate(C(i) = = maximum
     C);
end
```

FCM clustering is performed via the FCM function. Starting from the average position of each cluster, it starts with a randomized estimation for the cluster centers. Following that, FCM awards a randomized parameter to each data point for each cluster (Zuluaga-Gomez et al. 2021). FCM locates cluster centers within a data set accurately and determines the level of involvement in each cluster by directly altering the clusters and member ratings for every data point. The goal of this iteration is to minimize an ideal solution that weighted by the data point's cluster membership and represents the distances between each series of data points and a cluster center.

2.3 Method of thresholding

Threshold techniques are among the most fundamental tools for picture segmentation. The intensity level of these picture pixels was used to classify them. The multilateral thresholds are the most popular kind of thresholding strategy. The process involves determining a threshold value (TH) that is considered appropriate. This TH value will not fluctuate in the direction of the picture. As shown in Eq. 1, using TH, a finalized image $x(i,j)$ may be created from the initial image $y(i{:}j)$,

$$x(i,j) = \begin{cases} 1, & \text{if } y(i,j) > TH \\ 0, & \text{if } y(i,j) < TH \end{cases} \quad (1)$$

The choice of TH is dependent on two factors: the degree of vascular patterns discernible on thermal pictures, which varies from patient to patient and is dependent on the IR camera's thermal resolution; and the contrasting quality of an image, which was improved through the use of

Fig. 4 Segmentation process

histogram scaling. The different properties of these images obtained from numerous sources meant that a pre-selected threshold failed to perform effectively in detecting the vascularity variance of all the pictures in this investigation (Mambou et al. 2018). An ideal threshold was established by assessing how well each threshold performed in spotting aberrant patterns on the images. For every image group, the resultant picture from various thresholds was examined using a trial-and-error method. Values were computed utilizing the ideal thresholds, as mentioned in the preceding section, and utilized as an input characteristic for the DCNN analysis.

2.3.1 ROI

The ROI in this paper is obtained from the initial mammography image comprising two alternative ways employing a DCNN. The first method for determining the ROI is to utilize circular contours as the boundary for the calculation. The with in DSM datasets are classified with a red contour, so these outlines are computed physically by analyzing the tumor's image pixels and applying them to remove the area.

The linked edges served as the basis for the ROI. This image received the morphologic operators close to make sure that each of the gaps was filled. Finally, gaps in the binary representation of the ROI shape were filled in using MATLAB's infill function to flood-fill the image. This produced a mask, as seen in Fig. 5, that was applied to the initial image for additional processing.

The initial step in producing a ROI is identifying the tumor area utilizing the TH, which is a value generated in proportion toward the red color pixels. Following considerable testing, the thresholds were demonstrated at 76 for all images, independent of tumor size. The largest region inside this boundary anywhere throughout image was then calculated, and the tumor was automatically cropped.

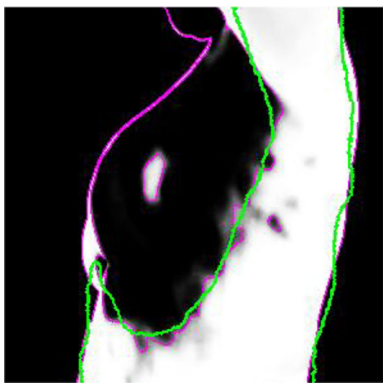

Fig. 5 ROI segment

2.3.2 *ROI method steps are as follows*:

1. Using threshold, convert the greyscale thermography to binary.
2. Labeling and counting binary picture pixels. All binary items are eliminated except the largest, the threshold calculated to identify tumor. The tumor's red outline is the finest region.
3. After the algorithm evaluated all binary input images, the pixels having the greatest area inside the threshold were assigned a value of one, "while the pixels with the smallest area were put to 0."
4. The generated binary image then combined with initial mammography image without consideration either remainder of the breast or abnormalities.

The center of the cluster is represented as a_0 and b_0. The image's width was changed by Eq. 2 to obtain different perspectives.

$$\left(\frac{a-a_0}{x}\right)^2+\left(\frac{b-b_0}{y}\right)^2=1 \tag{2}$$

However, because of the breast's position, the image was frequently distorted. Thus, rotation of the image is defined by degree of an angle as θ as given in Eq. 3.

$$\left(\frac{(a-a_0)\sin\theta+(b-b_0)\cos\theta}{x}\right)^2 + \left(\frac{(a-a_0)\cos\theta+(b-b_0)\sin\theta}{y}\right)^2=1 \tag{3}$$

The formulas were utilized to calculate each width factor and then identify each longitude line's index. A region that was possibly overlooked because it was so close to the ROI's edge may have been evident in an alternate image of the breast because it was scanned from eight distinct perspectives.

2.4 Feature extraction

Feature Extraction collects image material for indexing and retrieval. Primitive or low-level picture attributes include color, texture, and form extraction. This work uses GLCM to extract second-order texture characteristics for picture motion estimation.

In numerical texture classification, texture characteristics are generated using the probability model of intensities at given image points.

Figure 6 shows feature extraction following data collection. Feature extraction extracts picture object attributes. Before feature extraction, the breast sample picture is transformed to greyscale to control brightness. GLCM algorithm extracts features. Feature extraction using edge

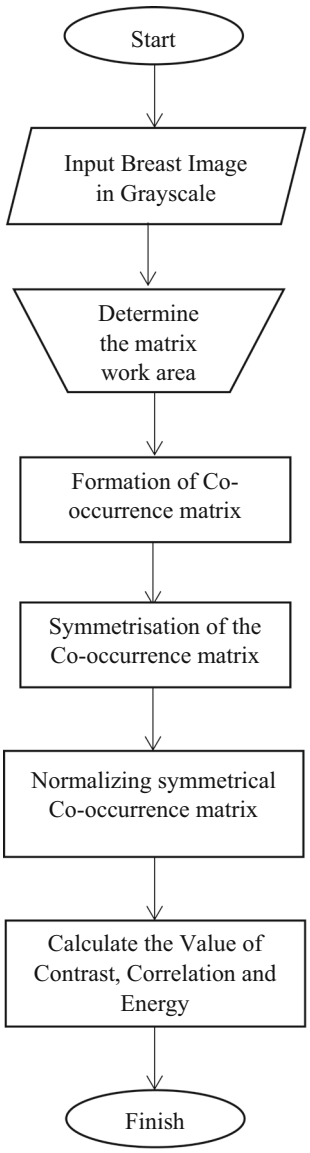

Fig. 6 Flowchart of feature extraction

detection is used to identify greyscale images. Image is retrieved based on entropy variables, intensity, radiation, and correlations. Each feature includes vital image data.

The GLCM matrix is a Nth-order matrix that describes the conditional probability probabilities of pixel pairings, where N is the image gray level. To minimize computational complexity and emphasize textural qualities, the picture gray level is often reduced to 8, 16, or 32 during the pre-processing step.

Frequencies in GLCM, $(\boldsymbol{P}(a,b;d,\theta))$ of concurrent occurrences of pixel $(a1,b1)$ and pixel $(a2,b2)$. Distance between pixel $(d1,d2)$ and pixel to the θ direction as shown in Eq. 4 and correlation is given in Eq. 5.

$$(\boldsymbol{P}(a,b;d,\theta)) = \#\left\{ \begin{array}{c} (a1,b1)(a2,b2)|c(d1,d2) = n| \\ (d1,d2) - P(a2,b2) = d = \theta \end{array} \right\} \tag{4}$$

$$CORRELATION = \sum_{i=1}^{n}\sum_{j=1}^{n} \frac{(x-\mu_i)(y-\mu_j)}{\sqrt{(\sigma_i)(\sigma_j)}} \tag{5}$$

where n is the total number of gray levels and $P(i, j)$ is the normalized greyscale value at positions i and j of a matrix with a total of 1. Textural characteristics were created using 100 greyscale photos. In this work, 48 textural characteristics were created for each greyscale picture, using distances between 1 as well as 2, angle at 0, 45°, 90°, and 135°.

When splitting the right as well as left breasts, each image is subjected to feature extraction, which identifies numerous features of the image, a few of which are listed below in Eqs. 6, 7, 8, and 9.

$$M = \frac{\sum^{f}(x)}{n} \tag{6}$$

$$V = \frac{\sum^{f}(x-M)^2}{n} \tag{7}$$

$$S = \frac{1}{n}\sum_{i=1}^{n}\sum_{j=1}^{n}\left(\frac{P(i,j)-\mu}{V}\right)^3 \tag{8}$$

$$K := \left\{\frac{1}{n}\sum_{i=1}^{n}\sum_{j=1}^{n}\left(\frac{P(i,j)-\mu}{v}\right)^4 - 3\right\} \tag{9}$$

where M is mean, V is variance, S is skewness, K is kurtosis.

Steps for feature extraction using GLCM

Input: Thermogrpahy image.
Output: Vector of textural features.
Begin
Step i: Calculate Grey level co—occurrence framework in four directions (0, 45, 90, 135) using d = 1.
Step ii: Normalize each GLCM matrix.
Step iii: for every GLCM matrix on a specific angle.
Step iv: Calculate texture equations.
Step v: Vectorize calculated features.
End

2.5 Image classification

A wide range of techniques available for the various categorization processes. The remarkable efficacy of deep convolutional neural networks, or DCNNs, has received a lot of interest recently. As a result of this, the Enhanced DCNN has been integrated into this paper.

2.5.1 EDCNN

In this research, EDCNN has been suggested as a method for the prognosis of the breast cancer diagnosis. The dataset found in the UCI repository was employed for the purpose of diagnosis, and GLCM was used for the extraction of features. A network takes as its inputs the final activations that it obtains from the previous convolution layer. After the first basic deep convolutional layer, a batch normalization layer as well as an activation function are applied using a mathematically convolution procedure respectively. To carry out a conveyor operation on each level using 20 one-dimensional filters, hyperparameters are utilized as shown in the string of 1, which shows how they are employed. This book makes use of the EDCNN architecture after it has been fine-tuned to categorize two categories rather than one thousand categories. A typical EDCNN will have three layers: a convolution layers, a pooling layer, as well as a fully-connected layers (fc) layer. The EDCNN architecture is produced when each of these layers is layered on top of one another. A comprehensive EDCNN model of each layer is shown in Fig. 7.

Minimizing the dimension of a Convolved Features feature is the responsibility of the pooling layers. Dimensionality reduction lowers the amount of computing power required to process the data. It is also useful for isolating translationally and lateral invariant dominant traits, which facilitates effective model training. The Fully linked layer and the Pooling Layer comprise an EDCNN's *n*-th layer. Raising the number of these layers can yield even more low-level information, but accomplishing so will require more processing power due to the complexity of the image. A Region Proposal Network (RPN) is a fully-connected network that correctly predicted object limits as well as bounding box coordinates scores at each place at the same time. In this case, feature selection is required for deep learning support since non-relevant features might influence deep-learning classification performance (Dharani and Bojja 2022). The feature selection improves classification accuracy while decreasing model time.

$$s^{(1)} = \rho(\omega^{(1)}\tilde{b} + a^{(1)}) \tag{10}$$

$$s^{(n)} = \rho(\omega^{(n)}s^{(n-1)} + a^{(1)}, \quad n = 1, 2, \ldots, m \tag{11}$$

As indicated in the preceding Eq. 10 and 11, (*n*) represents the distance matrix, hidden vector, as well as biased vector in the ith layer, where n denotes the degree of layers and ρ denotes the activation function.

An EDCCN, every input variables (*a*1, *a*2, *a*3, and *an*) is increased by a weight value *x* before being added together (Eq. 12). The cumulative value will be used as the activation function's input: *f*(*D*).

$$N_{x,a}(D) = f(X^n a) = f\left(\sum_{i=1}^{n} x_i + a\right) \tag{12}$$

As the activation function, choose the sigmoid function (one of the convolution layers widely used in deep-learning models) (Dharani 2019). (Eq. 13):

$$f(x) = \frac{1}{1 + e^{-x}} \tag{13}$$

Equation 14 is used to compute overall output with this layer.

$$\text{conv layer} = \left(\frac{\text{input} - \text{filter size}}{\text{Stride}}\right) + 1 \tag{14}$$

computing overall pooling layer shown in Eq. (15).

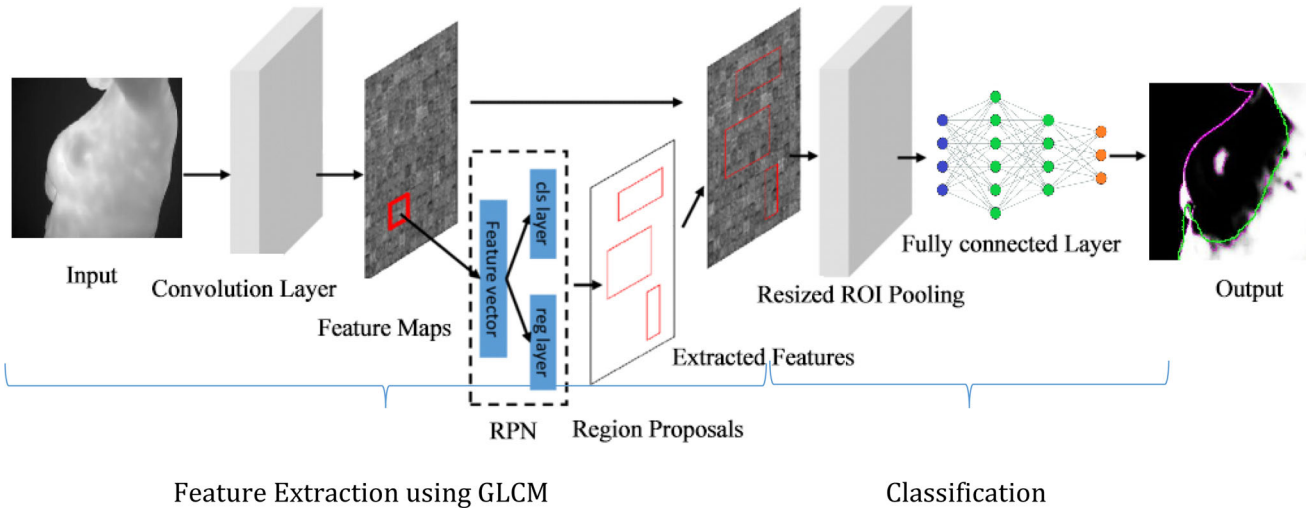

Fig. 7 EDCNN Model for detecting breast cancer

$$\text{pooling layer} = \left(\frac{\text{output of conv} - \text{pool size}}{\text{Stride}}\right) + 1 \quad (15)$$

3 Results and discussion

3.1 Dataset description

The DMR datasets contains mainly clinical data obtained from approximately1000 thermogram images gathered from Visual Labs. Thermograms evaluation, information on diagnosing throughout 1 year, patient age, previous history of tumors, diagnostic information, breast density, and all part of the clinical data. The pre-processing technique for our collected datasets are shown in Fig. 8.

Morphologic procedures used a complex structure to produce an outcome image the parallel dimensions as the input picture. The morphologic operations calculate the values of every pixel in the outcome image by contrasting it with its neighbor image pixels, as shown in Fig. 9, and indexing image iteration is illustrated in Fig. 10.

It is essential to make a diagnosis as well as to visually locate the tumor in the thermal imaging. The suspected tumor regions are indeed vital to the segmentation with epoch loss for the purpose of providing an appropriate diagnostic of malignancy based on thermograms. As seen in Fig. 11, this produced a mask that was applied to the initial picture for 400 rounds of additional processing (Fig. 12).

Pixel value as from chest area comprise the group with the highest peak at the lowest pixel value. In fact, this distinct luminance contrast between the chest area as well as the background is apparent in all of the images as shown in Fig. 13. Increasing the pixels density of the chest area to span the whole intensity range may improve these images.

Figure 13a, b provides features extractions parameter utilizing the grey-level co-occurrence matrix (GLCM) technique. These parameters are crucial for characterizing the texture and patterns within the thermal images. Contrast (0.23) measures the variation in intensity between neighboring pixels, reflecting texture differences.

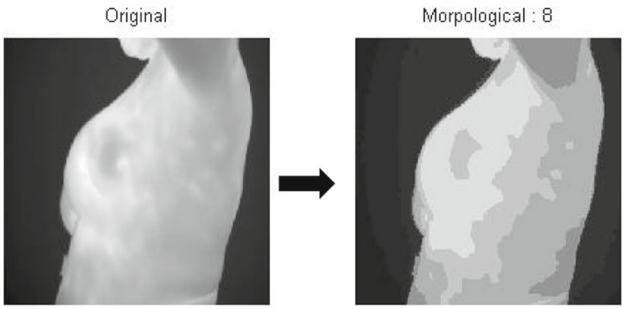

Fig. 9 Morphologic analysis

Correlation (0.93) assesses the linear dependency between pixel values, indicating the degree of uniformity or linearity in the image. Energy (0.18) quantifies the uniformity and complexity of the texture; higher values indicate more uniformity. Homogeneity (0.93) gages the closeness of pixel pairs, emphasizing the similarity in texture. Mean (0.43) and Standard Deviation (SD) (0.46) signify the image's central tendency and variation. Entropy quantifies the level of disorder or randomness in the image, with a value of 0.37, indicating moderate disorder. RMS (Root Mean Square) at 0.56, it represents the image's overall intensity, capturing variations in pixel values. Variance With a value of 0.14, it measures the spread of pixel values, indicating relatively low variability. Smoothness at 0.98, it suggests a high degree of homogeneity or uniformity in the image texture. Kurtosis (Kurt) at 1.14, it characterizes the shape of the histogram, indicating the peakedness or flatness of pixel value distributions. Skewness (Skew): With the value of 0.34, it measures the asymmetry of the pixel values distributions. These parameters play a significant role in quantifying textural attributes within thermal images, contributing to the diagnostic accuracy of the breast cancer detection system.

The variance between the output picture and the targeted picture is the basis for computes the error. The mean squared error (MSE) is the next statistic to be computed as shown in Fig. 14.

When compared with the entire breast image, the proposed method predicts an accurate classification of malignancy as well as benign cancers as shown in Fig. 15.

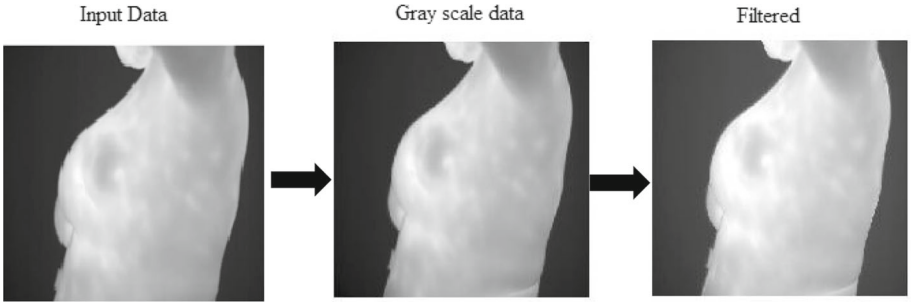

Fig. 8 Pre-processing technique

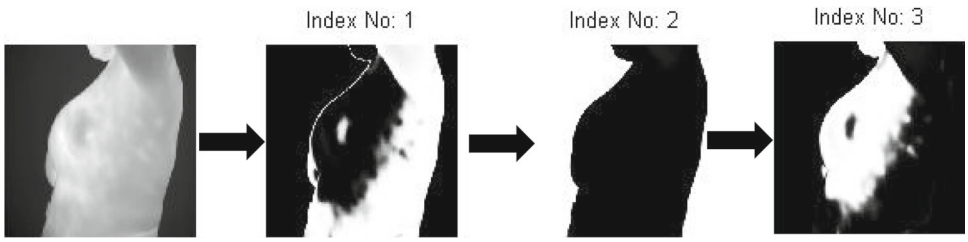

Fig. 10 Indexing images with Iteration

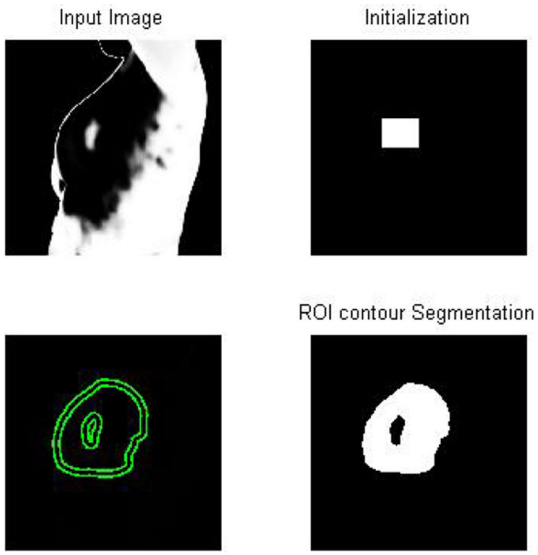

Fig. 11 Segmentation process

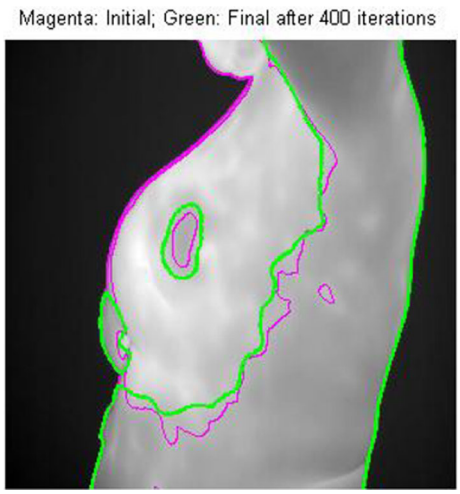

Fig. 12 ROI contour segmentation process

Figure 16 presents a comparative analysis of execution times between two image processing models: CNN and EDCNN, using a set of five images. It is evident that the EDCNN consistently outperforms the CNN in terms of execution time for all five images. In each case, EDCNN demonstrates a faster processing speed, with execution times ranging from 21.1 to 22.5 s, while the CNN lags slightly behind, with execution times between 23.1 and 24.3 s. This comparative analysis highlights the efficiency and speed advantage offered by the EDCNN over the traditional convolutional neural network (CNN) for processing thermal breast images, which is critical for real-time diagnostic applications and timely medical interventions.

Figure 17 offers a comparative analysis of the accuracy achieved by two image processing models, CNN and EDCNN, across a set of five images. Notably, the EDCNN consistently outperforms the CNN in terms of accuracy across all five images. In each case, EDCNN exhibits a higher accuracy percentage, ranging from 95.5 to 96.8%, while the CNN falls slightly behind, with accuracy percentages ranging from 91.8 to 93.9%. This comparison underscores the EDCNN as a more accurate and reliable tool for breast cancers' diagnosis utilizing thermal pictures. The difference in accuracy is substantial, highlighting the significance of EDCNN in enhancing diagnostic precision and potentially reducing false diagnoses.

Figure 18 offers a distinct perspective on the performance of CNN and EDCNN, focusing on specificity across a set of five images. Once again, EDCNN consistently demonstrates superior performance compared to CNN. Specificity values for EDCNN range from 92.7 to 93.7%, while those for CNN range from 90.7 to 91.9%. Specificity is a critical metric in medical applications, representing the model's ability to correctly identify true negatives, which are non-cancer cases, thereby reducing false alarms and ensuring reliable diagnoses. The EDCNN's higher specificity values highlight its effectiveness in minimizing the risk of false alarms and, consequently, increasing the overall reliability of breast cancer diagnosis using thermal images. This underscores the practical significance of EDCNN in the medical field.

The discussion encompasses the key methods employed in this study to enhance breast cancer detection using thermal images. The dataset, collected from DMR, is rich in clinical information, offering valuable diagnostic insights. A robust pre-processing technique involving morphologic operations and image iteration was used to prepare the data for further analysis, enabling the effective segmentation of suspicious tumor regions. Features extractions through the GLCM (greylevel co-occurrence matrix) technique extracted vital texture-related parameters

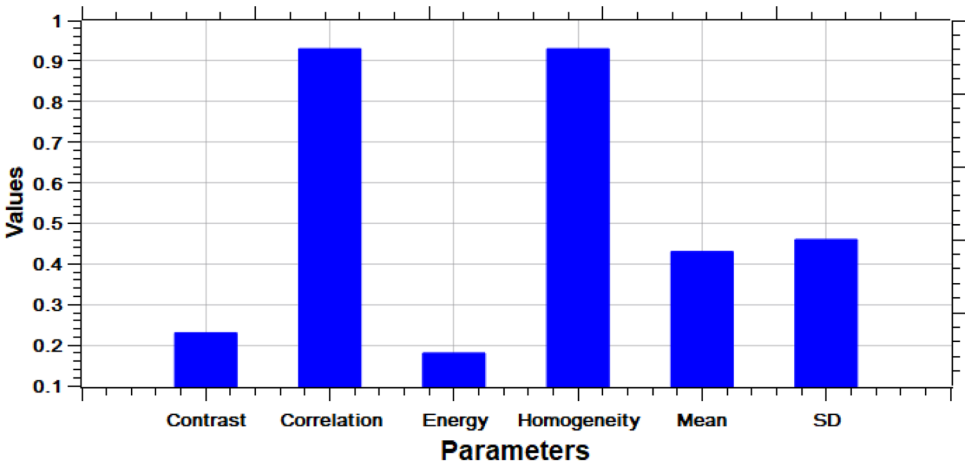

a) Feature Extraction Parameters using GLCM method

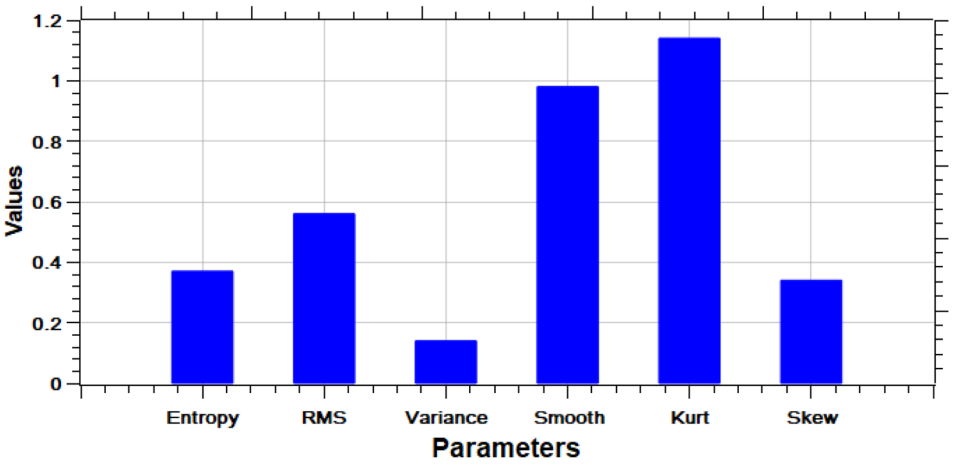

b) Feature Extraction Parameters employing GLCM method

Figure13 **a** Feature extraction parameters using GLCM method. **b** Feature extraction parameters employing GLCM method

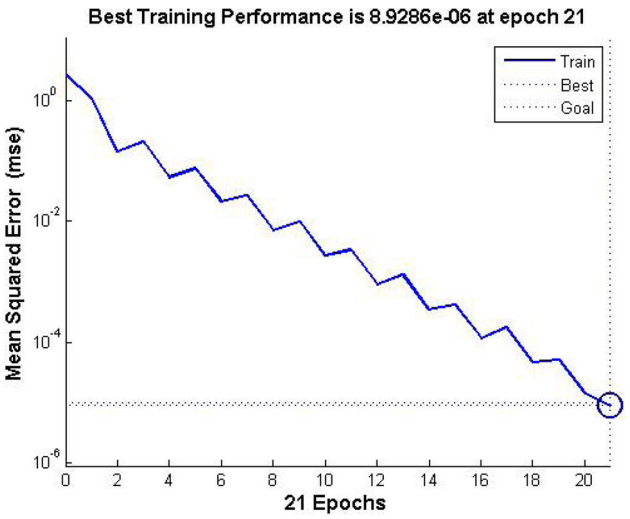

Fig. 14 Mean squared error with epochs

that play a crucial role in characterizing breast tissue abnormalities. The EDCNN outperformed the traditional

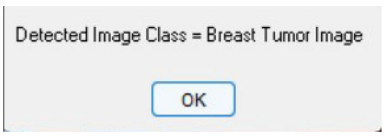

Fig. 15 Classification of an image using EDCNN

convolutional neural network (CNN) in terms of accuracy, speed, and specificity, as evidenced by comparative analyses. These findings illustrate the superior performance of EDCNN in breast cancer diagnosis, with higher accuracy and specificity, minimizing false alarms. The ability of EDCNN to provide faster results is pivotal in real-time clinical settings. These methods collectively contribute to a more accurate, efficient, and reliable system for early breast cancer detection using thermal imaging, showcasing the practical significance of this research in the field of medical diagnostics.

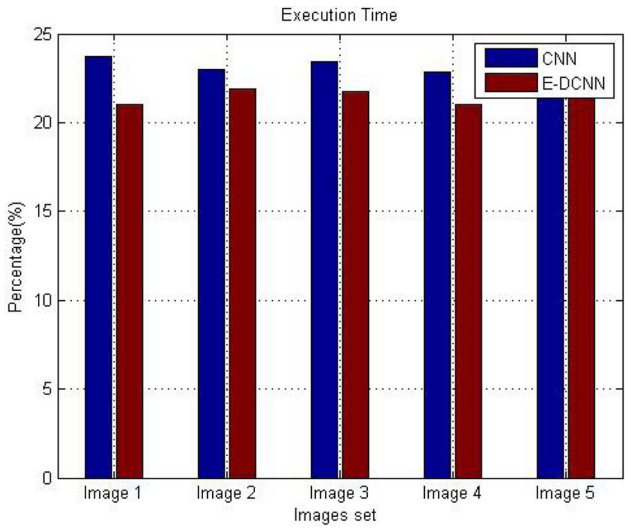

Fig. 16 Comparison of execution time

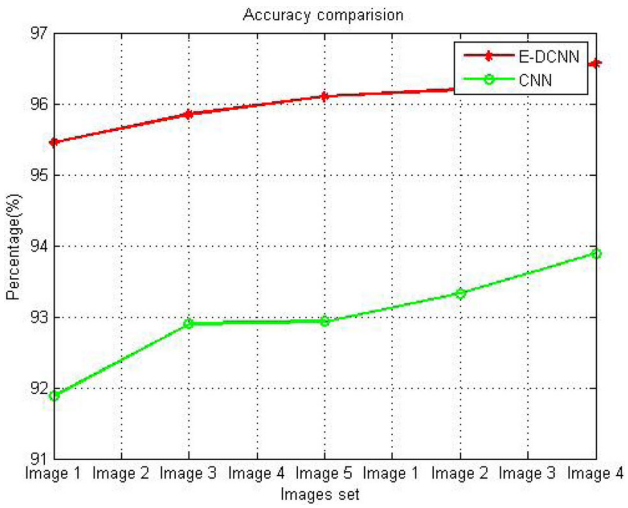

Fig. 17 Accuracy comparison for CNN versus EDCNN

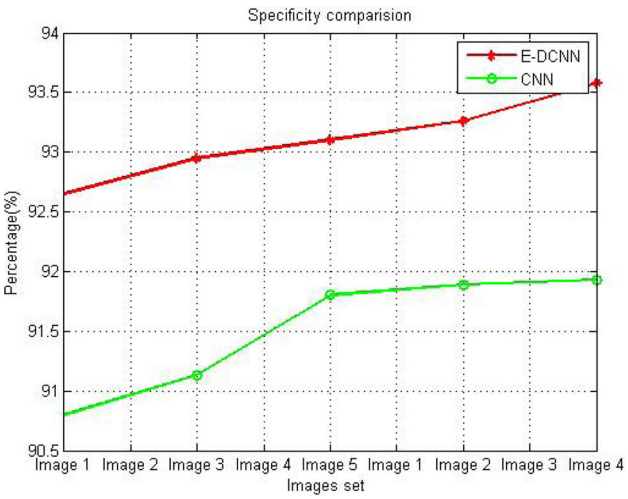

Fig. 18 Specificity comparison

4 Conclusion

In conclusion, this research aimed to develop an advanced diagnostic system for breast cancer using thermal images, with a primary focus on enhancing accuracy, efficiency, and early detection capabilities. To achieve this, we proposed two segmentation techniques, one involving circular contours and the other utilizing a region-based approach, both effectively isolating Regions of Interest (ROIs). Features extractions with GLCM (grey-level co-occurrence matrix) and image classification using enhanced deep-learning-based convolutional neural networks (EDCNN) significantly increased accuracy of diagnostic, outperforming traditional CNN. This outcome addresses the core research questions, affirming that our approach can indeed enhance the precision and effectiveness of breast cancer detection through thermal imaging. However, our study has certain limitations, primarily focusing on thermal images. Future research directions should explore the integration of multiple imaging modalities to provide a more comprehensive assessment of breast cancer. In addition, the requirement for square images in the EDCNN model might limit its applicability to various image sizes and formats. These limitations suggest promising avenues for further investigation and development. Overall, this research contributes significantly to the field of breast cancer diagnosis through thermal imaging. The EDCNN model's enhanced accuracy and efficiency hold promise for practical clinical applications, potentially leading to earlier and more reliable breast cancer diagnoses. This work represents a vital step in the ongoing endeavors to refine and expand diagnostic capabilities, ultimately benefiting patient outcomes and healthcare practices.

Acknowledgements There is no acknowledgment involved in this work.

Author contributions All authors are contributed equally to this work.

Funding No funding is involved in this work.

Data availability Data sharing not applicable to this article as no datasets were generated or analyzed during the current study.

Declarations

Conflict of interest Conflict of interest is not applicable in this work.

Ethics approval and consent to participate No participation of humans takes place in this implementation process.

Human and animal rights No violation of Human and Animal Rights is involved.

References

Ahmed E (2022) unet database.rar. figshare. Dataset. https://doi.org/10.6084/m9.figshare.21225386.v1

Al Husaini MAS, Habaebi MH, Gunawan TS, Islam MR, Elsheikh EA, Suliman FM (2022) Thermal-based early breast cancer detection using inception V3, inception V4 and modified inception MV4. Neural Comput Appl 34(1):333–348

Allugunti VR (2022) Breast cancer detection based on thermographic images using machine learning and deep learning algorithms. Int J Eng Comput Sci 4(1):49–56

Chatterjee S, Biswas S, Majee A, Sen S, Oliva D, Sarkar R (2022) Breast cancer detection from thermal images using a Grunwald–Letnikov-aided Dragonfly algorithm-based deep feature selection method. Comput Biol Med 141:105027

Dar RA, Rasool M, Assad A (2022) Breast cancer detection using deep learning: datasets, methods, and challenges ahead. Comput Biol Med 2022:106073

Darabi N, Rezai A, Hamidpour SSF (2021) Breast cancer detection using RSFS-based feature selection algorithms in thermal images. Biomed Eng Appl Basis Commun 33(03):2150020

Dharani NP (2019) Detection of breast cancer by thermal based sensors using multilayered neural network classifier. Int J Eng Adv Technol 9(2):1

Dharani NP, Bojja P (2022) Analysis and prediction of COVID-19 by using recurrent LSTM neural network model in machine learning. Int J Adv Comput Sci Appl (IJACSA). https://doi.org/10.14569/IJACSA.2022.0130521

Ensafi M, Keyvanpour MR, Shojaedini SV (2022) A New method for promote the performance of deep learning paradigm in diagnosing breast cancer: improving role of fusing multiple views of thermography images. Health Technol 2022:1–11

Hakim A, Awale RN (2020) Thermal imaging-an emerging modality for breast cancer detection: a comprehensive review. J Med Syst 44(8):1–18

Karthiga R, Narasimhan K (2021) Medical imaging technique using curvelet transform and machine learning for the automated diagnosis of breast cancer from thermal image. Pattern Anal Appl 24(3):981–991

Mambou SJ, Maresova P, Krejcar O, Selamat A, Kuca K (2018) Breast cancer detection using infrared thermal imaging and a deep learning model. Sensors 18(9):2799

Mashekova A, Zhao Y, Ng EY, Zarikas V, Fok SC, Mukhmetov O (2022) Early detection of the breast cancer using infrared technology—a comprehensive review. Therm Sci Eng Progress 27:101142

Mishra S, Prakash A, Roy SK, Sharan P, Mathur N (2020, March) Breast cancer detection using thermal images and deep learning. In: 2020 7th international conference on computing for sustainable global development (INDIACom). IEEE, pp 211–216

Patra A, Behera SK, Barpanda NK, Sethy PK (2022) Two-layer deep feature fusion for detection of breast cancer using thermography images. Onkol Radiother 16(8):6–8

Ragab M, Albukhari A, Alyami J, Mansour RF (2022) Ensemble deep-learning-enabled clinical decision support system for breast cancer diagnosis and classification on ultrasound images. Biology 11(3):439

Sánchez-Cauce R, Pérez-Martín J, Luque M (2021) Multi-input convolutional neural network for breast cancer detection using thermal images and clinical data. Comput Methods Programs Biomed 204:106045

Torres-Galvan JC, Guevara E, Kolosovas-Machuca ES, Oceguera-Villanueva A, Flores JL, Gonzalez FJ (2022) Deep convolutional neural networks for classifying breast cancer using infrared thermography. Quant InfraRed Thermogr J 19(4):283–294

Tsietso D, Yahya A, Samikannu R (2022) A review on thermal imaging-based breast cancer detection using deep learning. Mobile Inform Syst 2022:1

Zadeh HG, Haddadnia J, Ahmadinejad N, Baghdadi MR (2016) Assessing the potential of thermal imaging in recognition of breast cancer. Asian Pac J Cancer Prev 16(18):8619–8623

Zuluaga-Gomez J, Al Masry Z, Benaggoune K, Meraghni S, Zerhouni N (2021) A CNN-based methodology for breast cancer diagnosis using thermal images. Comput Methods Biomech Biomed Eng Imaging Visual 9(2):131–145